PRAMANA
— journal of
physics

Vol. 57, Nos 5 & 6
Nov. & Dec. 2001
pp. 1139–1161

Spatial solitons in nonlinear liquid waveguides

R BARILLÉ and G RIVOIRE
Laboratoire des Propriétés Optiques des Matériaux et Applications/CNRS - Université d'Angers,
4, Boulevard Lavoisier, B.P. 2018, 49016 Angers Cedex, France
Email: regis.barille@univ-angers.fr

Abstract. Spatial solitons are studied in a planar waveguide filled with nonlinear liquids. Spectral and spatial measurements for different geometries and input power of the laser beam show the influence of different nonlinear effects as stimulated scatterings on the soliton propagation and in particular on the beam polarization. The stimulated scattering can be used advantageously to couple the two polarization components. This effect can lead to multiple applications in optical switching.

Keywords. Nonlinear waveguide; stimulated Rayleigh wing scattering; soliton; polarization switch.

PACS Nos 42.65.Es; 42.65.Tg; 42.65.Wi

1. Introduction

What is spatial evolution of a laser beam travelling in a nonlinear medium? Diffraction occurs of course, like in the linear range, and tends to create a spatial spreading of the beam. Additive refraction phenomena, proper to the nonlinear range, are created by the light beam itself. When the refractive index n increases with the light density power per unit surface I, it yields a self-focusing of the beam [1]. Diffraction and self-focusing are in competition. Can we hope to reach a situation in which diffractional divergency is just compensated by nonlinear self-focusing?

1.1 *History*

In the early times of laser sources, the formation of laser self-trapped filaments in nonlinear media was observed [2]. In the output, transverse section of a laser beam, after its travel in a nonlinear medium such as CS_2, several bright spots are observed (figure 1). They display nearly the same diameter δ. These spots are the trace in the wave plane of laser filaments parallel to the propagation direction, keeping the same transverse size during their propagation. Observations of the longitudinal extension of these filaments have been made using either the transverse scattered light or partial reflectors displayed in the nonlinear liquid [3, 4]. This extension is currently of several centimeters in the experimental conditions described in figure 1. The number and positions of the filaments vary at random from one laser shot to another, and depend on the local spatial fluctuations of the laser intensity [5].

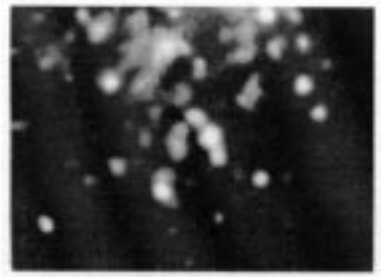

Figure 1. Laser beam transverse section at the output of a CS_2 cell (length 16 cm). Excitation provided by a *Q*-switch ruby laser (duration 30 ns) – mean intensity: 10 MW/cm^2. From ref. [5].

Figure 2. Laser beam transverse section at the output of a CS_2 cell (length 0.5 cm) – excitation provided by a mode-locked Nd:YAG laser (duration 30 ps). Intensity ranging from 3 MW/cm^2 to 3 GW/cm^2.

Several authors tried to control the formation of the filaments during their propagation in a bulk medium, and especially to build a single stable filament. This was obtained mainly using a focused unimodal laser, with a diffraction-limited divergency and an appropriate power [6]. Figure 2 illustrates this result. The appropriate power necessary to build a filament can be calculated using the following simplified model [1]:

The filament is considered as a self-guided light beam of diameter δ, in which light is confined due to the exact compensation of diffraction by self-focusing. This compensation is supposed to be reached when the total reflection limit angle θ_r is just equal to the diffraction angle θ_d. If we consider a laser intensity I constant in all the filament cross section, it yields a uniform nonlinear refraction index change Δn. Thus:

$$\theta_r = \sqrt{\frac{2\Delta n}{n_0}} = \theta_d = \frac{0.61\lambda}{n_0\delta}, \tag{1}$$

where λ is the light wavelength in vacuum and n_0 the linear refractive index at this wavelength.

The refractive index change is supposed to be connected to laser intensity by the relation (2):

$$\Delta n = n_2 I, \tag{2}$$

where n_2 is a constant characterizing the nonlinearity of the material. Thus, relation (1) yields:

$$P_{\rm cr} = \frac{\pi\delta^2}{4} I_{\rm cr} = \frac{(0.61\lambda)^2\pi}{8 n_0 n_2}, \tag{3}$$

where $P_{\rm cr}$ and $I_{\rm cr}$ are respectively the power and intensity of the laser beam contained in a filament. It is remarkable that the model gives no information on the size δ. It allows the calculation of the input beam power $P_{\rm cr}$ to obtain a self-trapped filament, but not the corresponding intensity $I_{\rm cr}$.

In the typical case of CS_2, $n_2 = 3.10^{-18}$ m^2/W, and thus $P_{\rm cr} = 7.6$ kW at the wavelength $\lambda = 0.5\ \mu$m.

In the experiments, δ is in the range 6 to 100 micrometers [7], according to the nonlinear material and to the presence of nonlinear absorption and of stimulated scatterings (Rayleigh, Raman) [8, 9]. These last ones have often been considered as processes limiting the decrease of the size of δ.

The research of stable solitons of the spatial Schrödinger nonlinear equation – ie of beams able to propagate without changes in their transverse intensity and phase distribution began in the seventies. Zakharov and Shabat [10] showed that the self-trapping stability requires propagation in two-dimensional (2D) media. In three-dimensional media (3D), solutions are unstable, in agreement with the experimental results reported above. The first evidence of solitonic propagation in 2D media –ie either in planar waveguides or in very thin beams, such as those produced in interference fringes – was reported in 1985 by Barhelemy, Maneuf and Froehly [11]. We now discuss briefly the origin of the 3D soliton instability, and, in doing this, we simultaneously discover some 2D soliton properties that we shall experimentally verify later on.

1.2 *On 2D and 3D solutions*

We consider the propagation in the z direction of a light beam described by the electric field $E(x,y)$. In the slowly varying envelope approximation, and in the absence of losses, the propagation equation is:

$$i\frac{\partial E}{\partial z} + \frac{1}{2k}\left[\frac{\partial^2 E}{\partial x^2} + \frac{\partial^2 E}{\partial y^2}\right] + kn_2|E|^2 E = 0, \tag{4}$$

where $k = (2\pi/\lambda)$. In the first member of eq. (4), the second term describes diffraction and the third one nonlinear refraction index change. Considering

$$E = \sqrt{HI}\,{\rm e}^{j\varphi}, \tag{5}$$

where H is a constant depending on the unit system, the phase φ and intensity obey:

$$\frac{\partial\varphi}{\partial z} = \frac{1}{2k}\left\{\frac{1}{2I}\left(\frac{\partial^2 I}{\partial x^2} + \frac{\partial^2 I}{\partial y^2}\right) - \frac{1}{4I^2}\left[\left(\frac{\partial I}{\partial x}\right)^2 + \left(\frac{\partial I}{\partial y}\right)^2 - \left(\frac{\partial\varphi}{\partial x}\right)^2 - \left(\frac{\partial\varphi}{\partial y}\right)^2\right]\right\} + kn_2 I, \tag{6a}$$

$$\frac{\partial I}{\partial z} = -\frac{1}{k}\left\{ I\left(\frac{\partial^2\varphi}{\partial x^2} + \frac{\partial^2\varphi}{\partial y^2}\right) + \frac{\partial\varphi}{\partial x}\,\frac{\partial I}{\partial x} + \frac{\partial\varphi}{\partial y}\,\frac{\partial I}{\partial y}\right\}. \tag{6b}$$

We look for a solitonic solution, i.e., for a phase (φ) independent of the transverse coordinates x and y. Equations (5) and (6) yield:

$$\frac{\partial\varphi}{\partial z} = \frac{1}{2k}\left\{\frac{1}{2I}\left(\frac{\partial^2 I}{\partial x^2} + \frac{\partial^2 I}{\partial y^2}\right) - \frac{1}{4I^2}\left[\left(\frac{\partial I}{\partial x}\right)^2 + \left(\frac{\partial I}{\partial y}\right)^2\right]\right\} + kn_2 I. \tag{7}$$

In eq. (7), $\partial\varphi/\partial z$ being independent of x and y can be considered as a constant called $C2$ or $C3$ respectively in the 2D and 3D cases. Introducing $r = (x^2 + y^2)^{1/2}$, eq. (7) can be written as follows:

$$C_3 = \frac{1}{2k}\left\{\frac{1}{2I}\left(\frac{\partial^2 I}{\partial r^2} + \frac{1}{r}\frac{\partial^2 I}{\partial r}\right) - \frac{1}{4I^2}\left[\left(\frac{\partial I}{\partial r}\right)^2\right]\right\} + kn_2 I. \tag{8}$$

For comparison, the 2D equation is:

$$C_2 = \frac{1}{2k}\left\{\frac{1}{2I}\left(\frac{\partial^2 I}{\partial x^2}\right) - \frac{1}{4I^2}\left[\left(\frac{\partial I}{\partial x}\right)^2\right]\right\} + kn_2 I. \tag{9}$$

Stable solutions exist for eq. (9). The first order one is obtained when constant $C2$ has the value C_{2S}, with:

$$C_{2S} = \frac{1}{2}kn_2 I_0. \tag{10}$$

This stable solution – called 2D first order soliton – obeys:

$$I = I_0 \frac{1}{ch^2(Kx)} \tag{11}$$

with

$$K = k\sqrt{n_2 I_0}. \tag{12}$$

This means that, in the 2D experiment, an intensity distribution described by expressions (11) and (12) propagates without deformation, with a phase obeying: $(\partial\varphi/\partial z) = (1/2)kn_2 I_0$.

Higher order solutions of (9) exist. They are not studied here.

Note that any intensity I_0 is convenient to build a soliton, provided that the beam shape and size obey relations (11) and (12). Figure 3a shows the solution of eq. (9) for the value $C_2 = C_{2S}$, ie the solution obtained in a planar structure. For comparison, solution of 3D eq. (8) in the case $C_3 = C_{2S}$ is shown in figure 3b, illustrating the strong difference between 2D and 3D structures.

The total soliton power in the soliton beam is:

$$P_s = d\int_{-\infty}^{+\infty} I(x)\mathrm{d}x = \frac{2dI_0}{K} = \frac{2d}{k}\sqrt{\frac{I_0}{n_2}}, \tag{13}$$

where d is the waveguide thickness, in the y dimension (see figure 4). The spatial half-width x_s of the soliton, defined by $I(x_s) = I_0/2$ is:

$$x_s = \frac{0.9}{K} = \frac{1.8d}{P_s k^2 n_2}. \tag{14}$$

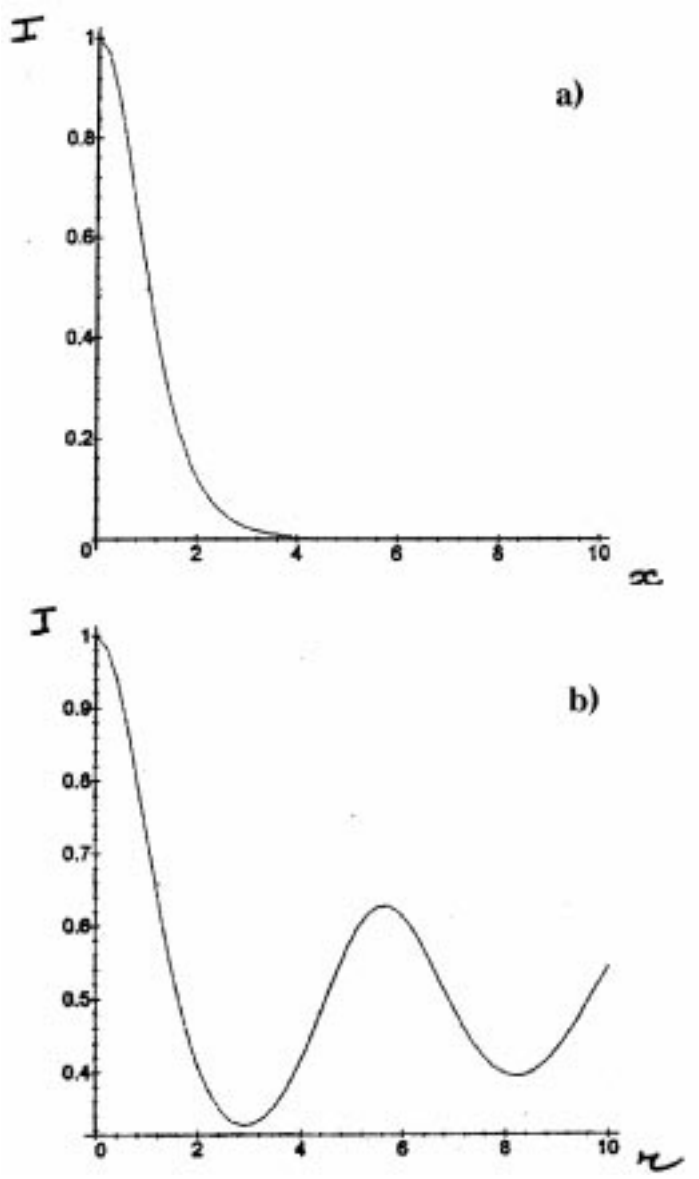

Figure 3. Solution of propagation equation: intensity I versus transverse dimension, (**a**) 2D soliton $(C_2 = C_{2S})$, (**b**) 3D solution $(C_3 = C_{2S})$.

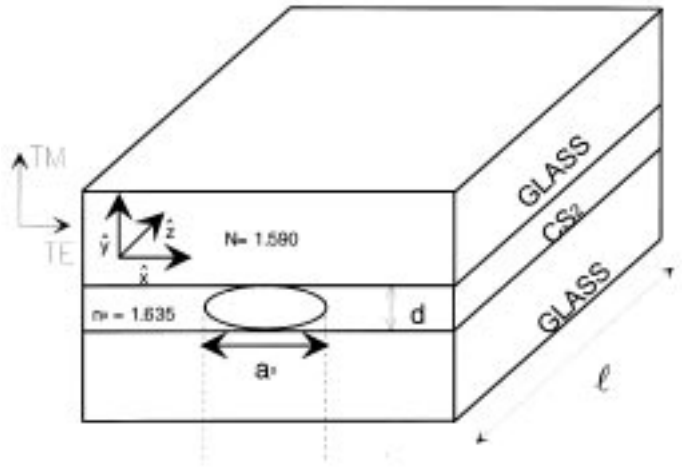

Figure 4. Liquid waveguide structure.

Usually, the beam size is imposed by the experimental set-up. In this case, a soliton can be obtained in a planar waveguide of thickness d, with an entrance size x_s, if two conditions are fulfilled:

1 - intensity distribution has the shape described by relation (11)

2 - total power in the beam is, from relation (14), total power in the beam is:

$$P_s = \frac{1.8d}{k^2 n_2 x_s}. \tag{15}$$

In CS_2, with: $d = 10\,\mu$m, $x_s = 100\,\mu$m, $\lambda = 532$ nm, $Ps = 400$ W, $d = 10\,\mu$m, $x_s = 10\,\mu$m, $Ps = 4000$ W.

We note that in formulas (14), (15), the numerical coefficient depends on the definition of the soliton width: it varies from 1.8 to 3.6 when the width is taken between $I_0/2$ and $I_0/10$. We shall later have the opportunity of experimental verifications of formula (15). We can compare the 2D soliton power P_s to the critical power $P_{\rm cr}$ (formula 3) necessary to build a 3D filament:

$$\frac{P_s}{P_{\rm cr}} = \frac{0.5d}{x_S}. \tag{16}$$

The ratio $P_S/P_{\rm cr}$ does not depend on the nonlinear material, but only on the geometrical dimensions. As, in experiments, $d \ll x_s$ (in order to assure a 2D structure), the soliton power will be usually much smaller than the critical power.

We go back now to the 3D solitonic equation (8). The term $\frac{1}{r}\frac{\partial I}{\partial r}$ in the second member of (8) – which is of diffractive origin – makes the difference with the 2D equation (9). It brings dissymmetry and instability. It is not our purpose here to study solutions of (8), but only to vizualize better the instability source term. Suppose we have found a solution of (8); the corresponding curve $I(r)$ has at least one inflexion point $\left(\frac{\partial^2 I}{\partial r^2} = 0\right)$ for coordinates r_i and I_i. The slope $(\partial I/\partial r) = u$ in this point obeys, from (8):

$$C_3 = \frac{1}{4kr_i}\frac{u}{I_i} - \frac{u^2}{8kI_i^2} + kn_2 I_i$$

i.e.,

$$u = \frac{I_i}{r_i}\left\{1 \pm [1 + 8r_i^2 k(kn_2 I_i - C_3)]^{1/2}\right\}. \tag{17}$$

In the 2D case, this slope would be (from (9)):

$$u = I[8k(kn_2 I_i - C_2)]^{1/2}. \tag{18}$$

Formula (18) shows that, in the 2D case, only one slope exists at the inflexion point (opposite values of u in x_i and $-x_i$), while in the 3D case two different values of the slope can exist for a same value of r_i, opening the door to a rupture of the cylindrical symmetry and to instabilities.

1.3 *Interest of nonlinear liquids*

2D planar waveguides can be either made of nonlinear solid such as nonlinear glass [12], or layer deposited on a convenient material [13], or made of a nonlinear liquid injected between two high refractive index plates [14]. Nonlinear liquid filled waveguides are very flexible tools because sizes d and x_s can be varied progressively and liquid can be changed. Absence of absorption and of birefringence contribute to making them interesting for verification of basic properties. But liquid planar waveguides are not only study tools. Their use in applications is envisaged, as shown by British Telecom and Hewlett-Packard [15].

We present a study of the main experimental results we obtained in the last few years in nonlinear liquid waveguides. Polarization properties are particularly attractive, opening the door to applications in the field of optical switching and limiting.

2. Spatial measurements

Our purpose is to verify the existence of 2D soliton in a planar waveguide, and to compare its power and geometrical parameters to those described in eqs (11), (12) and (15).

Experiments are made with the waveguide described in figure 4. Its length is $l = 5$ cm. Excitation is provided by a Nd:YAG laser delivering 30 ps pulses at the wavelength $\lambda = 532$ nm. In the first experiments, polarization of the input beam is either TE or TM. The waveguide is filled with CS_2, which is a classical reference transparent nonlinear liquid. The input beam is shaped by a combination of cylindrical and spherical lenses to the dimensions d and a. Figure 5a shows the input intensity distribution. The output shape is measured by imaging the exit face of the waveguide on a CCD camera. Results are shown in figure 5b, for increasing values of the entrance power P. At low power, the beam is large, due to diffraction along the x dimension. Then, its size is reduced and becomes equal to the input size: the soliton is obtained at a power $P = Ps$. With a further increase of P, self-focusing dominates, and filamentation appears. For instance, with $d = 8\ \mu$m, $a = 52\ \mu$m, a first filament is created at $P \approx 2.2P_S$, with a size $x_{\text{out}} = 20\ \mu$m. With further increase of P, several filaments appear, with the same limit size, but their positions vary laterally at random [16].

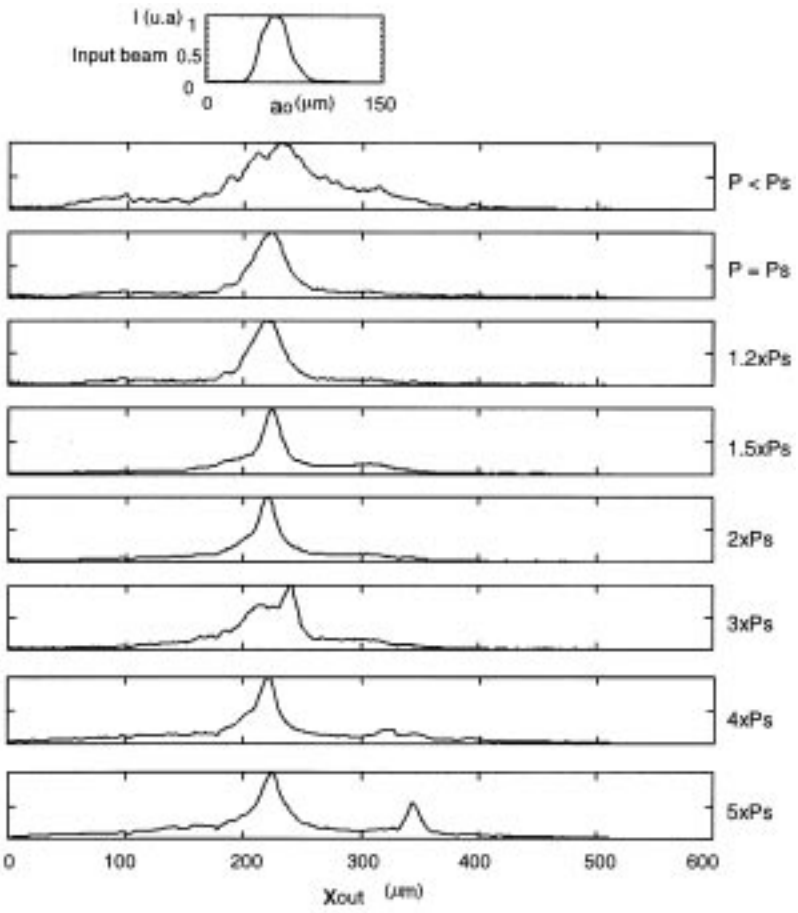

Figure 5. Spatial evolution of the output beam with input power P. Intensity in arbitrary units versus dimension x. (**a**): entrance beam, (**b**): output beam for increasing values of P.

We remark that we have not tried to obtain with great precision the hyperbolic secant shape (formula 11) for the input beam. This shape is relatively close to the Gaussian one (figure 6) generally delivered by the lasers. It is an experimental matter of fact that spatial soliton is not sensitive to small laser shape fluctuations.

Comparison between measured and calculated values of P_s shows a good agreement. For instance with $a = 52\ \mu$m, $d = 8\ \mu$m, we measure in the TE polarization a soliton power of 2.3 kW. From formula (15), we calculate 1.4 kW, however, in the measurement, size a is measured at $I_0/10$ (see figure 5a), and, in the y dimension, intensity is not uniform but nearly Gaussian. This imposes a double numerical correction in the calculation of P_s; instead of coefficient 1.8 in (15), we have to take 2.7 and thus the calculated value of P_s is 2.1 kW. For the TM polarization some instabilities appear; the soliton power is higher than in TE polarization; this question will be discussed later. The influence of the soliton

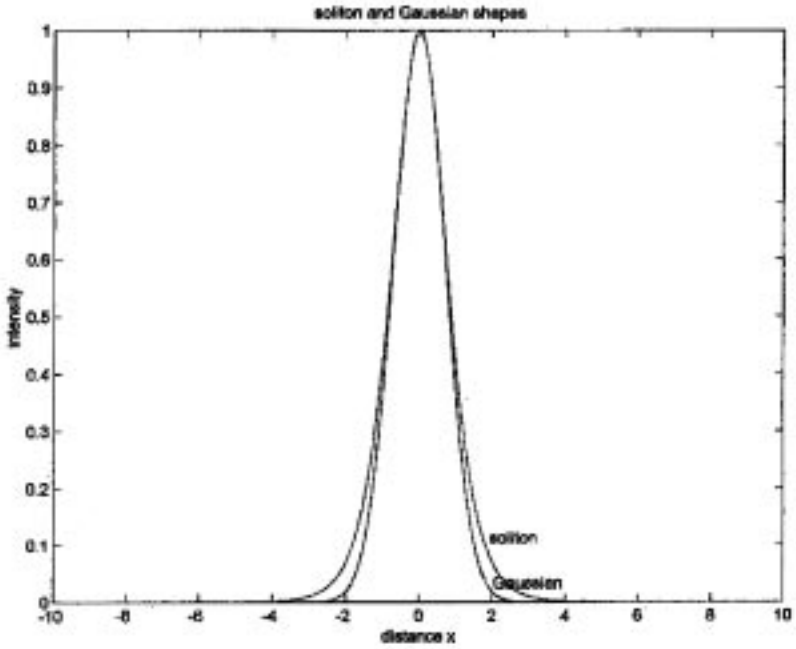

Figure 6. Comparison between soliton and Gaussian shapes of transverse intensity versus distance to the beam center.

dimensions d and $a = 2x_s$ on the soliton power P_s has been studied. Typical results are shown in figure 7 [17]. P_s is proportional to d/x_s, in agreement with formula (15).

As concerns the creation of self-trapped filaments we observe that the critical power in a filament is smaller in the waveguide than in the bulk. For instance, in bulk CS_2, we have measured $P_{cr} = 8.5$ kW [18], while in the guide we measure $P_{cr} = 2.2Ps = 5$ kW. The bulk measured value agrees with the calculated one (formula 3). Thus, the presence of the guiding structure diminishes the critical power. Moreover, the filament size δ is smaller in the bulk ($\delta = 6\ \mu$m [18]) than in the waveguide ($\delta = 20\ \mu$m). Thus, the intensity in a filament is far larger in the bulk than in the guide (ratio of the order of ten or more). We want to note here that in bulk stabilized self-trapping, only a part of the laser power is concentrated in the filament (of the order of 10 % in ref 18), while in 2D soliton, nearly all the entrance power in guided.

3. Spectral measurements

Equations presented previously (in introduction) hold for stationary temporal situation. In this case, the input and output light spectra are identical. However, in experiments, illumination is provided by short laser pulses and in nonlinear media spectral modifications can be expected due to phase modulation (PM).

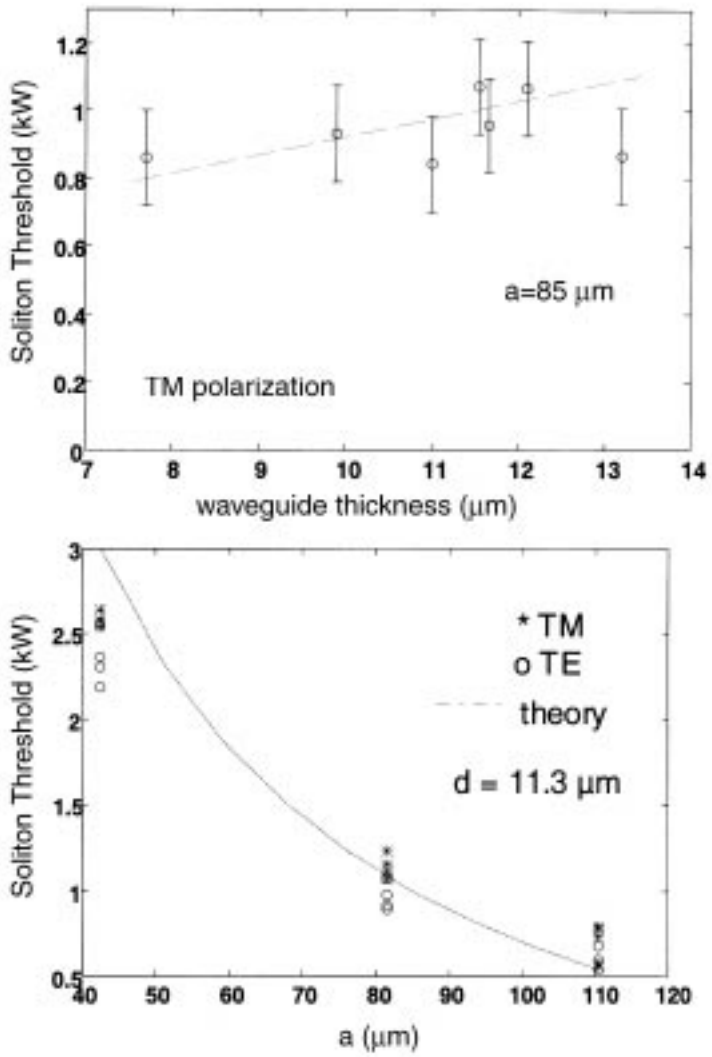

Figure 7. Influence of the size parameters d, a on the solitonpower Ps. (**a**) Ps versus d for $a = 85$ μm (- - - : theoretical curve) (**b**) Ps versus a for $d = 11.3$ μm (___: theoretical curve).

De facto, in the picosecond range, spectral changes are observed, depending on the entrance power. Figure 8 illustrates these changes [16]. An image of the output face of the waveguide is made on entrance slit of a spectrometer, the slit being parallel to the x axis (defined on figure 4). Thus in spectra presented in figure 8, the vertical size demonstrates the spatial components of the output beam: strong spectral changes appear in the central part of the beam, while in the very low intensity wings, there is no spectral broadening. This wing part can therefore be used as a spectral refence of the input laser.

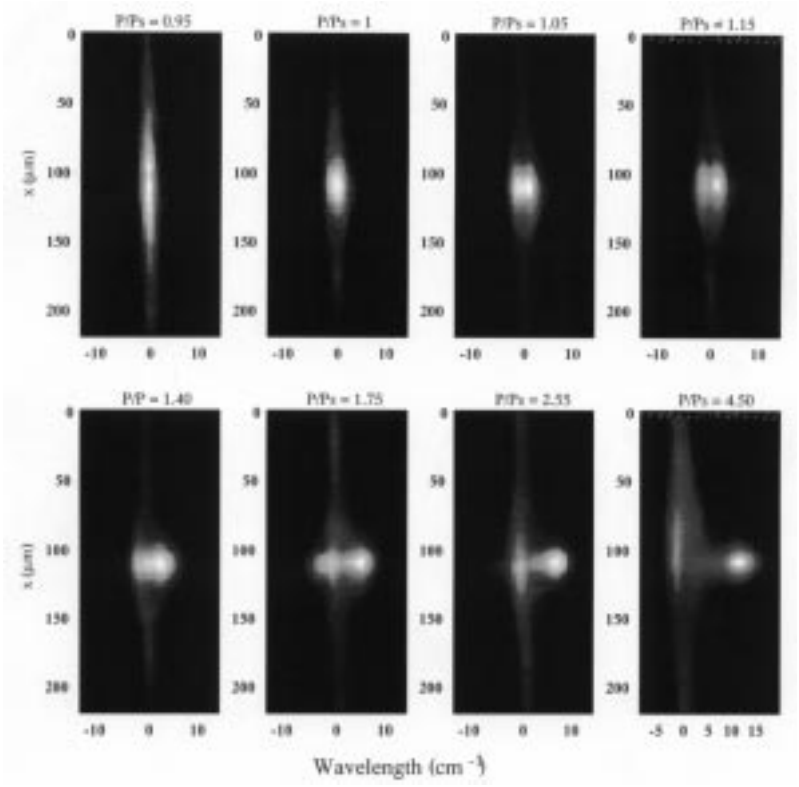

Figure 8. Spectral evolution with th input power. Point zero of the wavelength axis refers to the laser line (18 797 cm^{-1}). $d = 12\ \mu$m, $a = 85\ \mu$m.

Before quantitatively analysing the results, we restate the main features characterizing PM. Nonlinear phase change φ of the electric field is proportional to I (from formula (2)), and thus for short pulses depends on time t. This yields a PM, that can be calculated representing the electric field $\mathscr{E}(t)$ through its Fourier transform $E(\omega)$ and writing $I(\omega) \approx |E(\omega)|^2$. For Gaussian temporal pulses, typical computer calculated modulation spectra are represented in figure 9. They are characterized by a Stokes/anti-Stokes symmetry, by the presence of a maximum of intensity at the extremities of the Stokes and anti-Stokes wings. The total spectral width is classically estimated by the formula [19]:

$$\frac{\Delta\sigma_{\mathrm{out}}}{\Delta\sigma_{\mathrm{in}}} = [1 + (0.88V)^2]^{1/2}, \tag{19}$$

where $\Delta\sigma_{\mathrm{in}}$ and $\Delta\sigma_{\mathrm{out}}$ are respectively the input and output spectral widths, and $V = 2\pi\ell n_2 I/\lambda$. The calculated value of $\Delta\sigma_{\mathrm{out}}$ in the soliton thus increases with the soliton intensity. This intensity can be calculated. From relations (13) and (15), the value Is of I_0 for a soliton size $a = 2x_s$ is:

$$I_s = \frac{3.2}{n_2 k^2 a^2}. \tag{20}$$

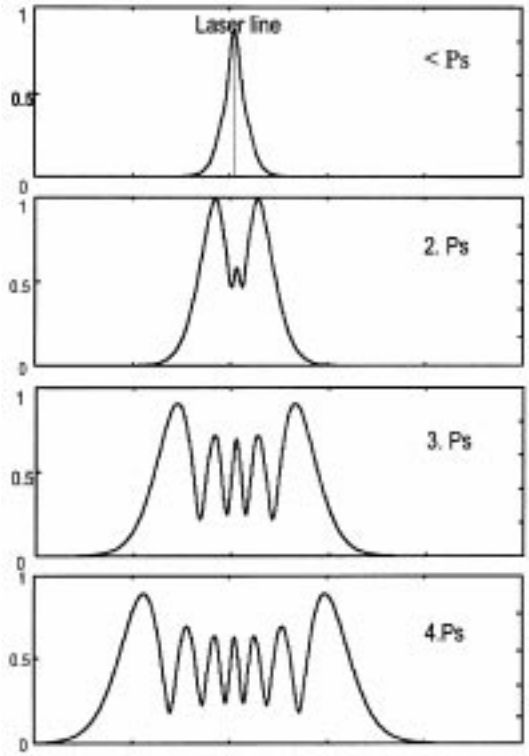

Figure 9. Calculated phase modulated spectrum ($a = 50\ \mu$m) for different values of power P.

This intensity depends strongly on the size a. Therefore, the spectral width $\Delta\sigma_{\text{out}}$ of the soliton is expected to depend on a. For instance, with $a = 40\ \mu$m, $Is = 0.48$ GW/cm^2 and thus $(\Delta\sigma_{\text{in}}/\Delta\sigma_{\text{out}}) = 8$, while with $a = 110\ \mu$m, $Is = 0.06$ GW/cm^2, $(\Delta\sigma_{\text{out}}/\Delta\sigma_{\text{in}}) = 14$.

The output spectra observed around the soliton power Ps, in the case of a linearly polarized TM input beam, are measured for the values $a = 40\ \mu$m, 80 μm, 110 μm [17].

In the three cases, the spectral width remains small for input powers smaller than Ps. The spectral broadening occurs near $P = Ps$. The influence of the power P on the total spectral width is shown in figure 10. Typical spectra are displayed in figure 11. The results can be summarized as follows:

- $a = 40\ \mu$m

  The soliton power is 2.4 kW (intensity $Is = 0.48$ GW/cm^2). At the soliton power, a small dip appears in the center of the laser line (figure 11). The spectral broadening increases with P. As soon as $P/Ps = 1.05$, the distance between the Stokes and anti-Stokes peaks reaches 10 cm^{-1}. The maximum of intensity is always obtained at the far red extremity of the spectrum (figure 11). The calculated value of $\Delta\sigma_{\text{out}}$, for $I = Is$, is 30 cm^{-1} (formula 19), in agreement with the measured one (figure 10). Thus, phase modulation can explain the spectral broadening observed in the small size soliton.

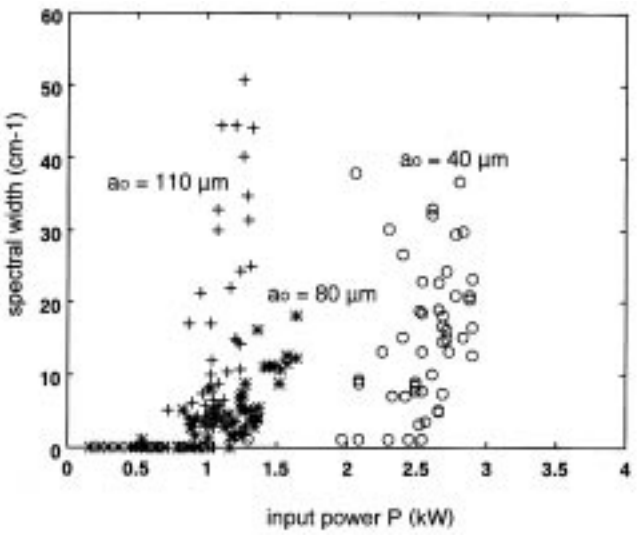

Figure 10. Total spectral width versus power P for 3 cases : $a = 40\ \mu$m ($Ps = 2.4$ kW), $a = 80\ \mu$m ($Ps = 1.2$ kW), $a = 110\ \mu$m ($Ps = 0.9$ kW).

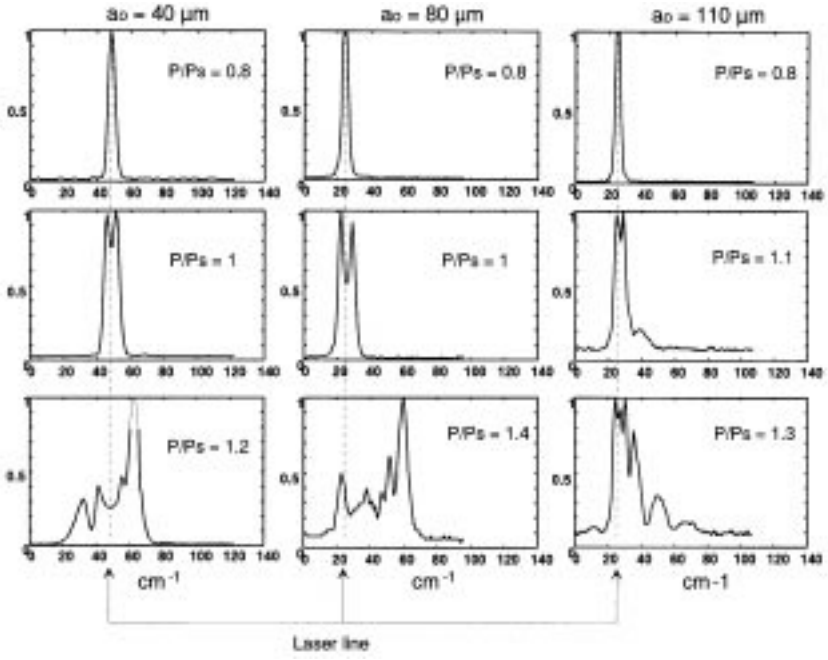

Figure 11. Spectral broadening at the output of the waveguide for different sizes a : intensity versus frequency.

- $a = 110\ \mu$m

  The soliton power is 0.9 kW ($I_s = 0.06$ GW/cm^2). The output line remains thin and symmetrical until $P/P_s = 0.96$. When P reaches the value $0.96P_s$, the line is broadened and presents one Stokes and one anti-Stokes peak on its sides, situated at the same distance ≈ 4 cm^{-1} of the laser line (figure 11). A large and sudden broadening occurs immediately above the soliton power. The spectral band shape is very different from that obtained in the case of the small size soliton: now, the intensity decreases from the laser frequency to the red spectral end, instead of showing a maximum at this red end (figure 11). The calculated value of $\Delta\sigma_{\text{out}}$ is much smaller than the measured one, implying that the spectral broadening is not due to PM.

- $a = 80\ \mu$m

  For this medium input size, the spectra are near those obtained when $a = 40\ \mu$m. The only difference is the presence of a more rich and regular line structure, the mean distance between the lines being in the range of 4 cm^{-1}.

  As we shall see later, the broadenings that are not explained by PM, particularly in the case of large values of a, are explained by the presence of stimulated Rayleigh wing scattering (SRWS). A brief description of this type of scattering is necessary for understanding its role in soliton propagation.

3.1 *Stimulated Rayleigh wing scattering (SRWS)* [1,20,21]

Rayleigh wing scattering is a type of scattering resulting from the tendency of anisotropic molecules to be oriented by a light field. Spontaneous Rayleigh wing scattering is amplified in strong exciting light field, providing stimulated scattering, like emission is amplified in lasers. A gain g can be calculated. It depends on the frequency distance Ω of the SRWS to the laser exciting line:

$$g = g_0 \frac{2\Omega\tau}{1 + \Omega^2\tau^2} \tag{21}$$

where τ is the molecular orientation relaxation time ($\tau = 2$ ps in CS_2), and g_0 the maximum value of g, obtained for $\Omega_0 = (1/\tau)$ (2.3 cm^{-1} in CS_2).

Molecular orientational movements driven by laser field are not only the source of SRWS, but also the source of nonlinear refractive index changes by Kerr effect. Gain g_0 and coefficient n_2 (defined in formula 2) are both proportional to the square of molecular anisotropy. Thus, it is normal to observe, with a strongly anisotropic molecule like CS_2, both Kerr effect and SRWS. In this liquid, 90 % of the constant n_2 has a Kerr origin, and only 10 % has an electronic origin. With isotropic molecules (like $CHCl_3$, that we use later on in this work), n_2 is only due to electronic cloud deformations and SRWS is thus absent.

Why do SRWS appears in the large size soliton, and not in the small size one, in the previous spectra (figure 11)? This is connected with the level of intensity threshold I_T of SRWS. If this threshold is larger than the soliton intensity I_s, SRWS does not exist in the soliton. As I_s depends on the soliton size a, we can understand why, changing a, we can change the influence of SRWS.

The threshold I_T can be estimated as follows: we suppose that SRWS intensity has an exponential increase described by $\exp(gI\ell)$. Threshold is reached when the quantity $G = gI\ell$ has a value of the order of 20. Thus, at $\Omega = \Omega_0$,

$$I_T = \frac{20}{g_0 \ell}. \tag{22}$$

In CS_2 $g_0 \approx 3 - 10$ cm/GW [20–22]. With $\ell = 5$ cm (case of the waveguide in figure 4), I_T is in the range 1.3 to 0.4 GW/cm^2. Threshold measurements in bulk CS_2 give values lower than these ones and situated between 0.06 and 0.1 GW/cm^2 [7, 22]. Thus the soliton intensity *Is* estimated above (from 0.06 to 0.48 GW/cm^2 according to the value of *a*) and the SRWS threshold I_T are in the same range of values in our experimental conditions. But while I_T is independent of the dimension *a*, *Is* depends on *a*.

Same kind of considerations can be developed for stimulated Raman scattering: its threshold – estimated by the same method as for SRWS – is independent of *a*. A convenient choice of parameters *a* and ℓ can rule the presence of absence of all the scatterings in solitons.

One more consideration must be added concerning SRWS. Due to the influence of the frequency change Ω on the gain, there exists a four photon process (FP) in which one Stokes and one anti-Stokes Rayleigh wing photons are created at the expense of two laser photons (elastic process). The efficiency of this FP coupling process depends on the wave vectors (phase matching) i.e., on the propagation directions of the involved beams. We have observed that in collimated beams [17, 23], the creation of Stokes SRWS by FP processes is particularly strong, and yields cascade effects: Stokes lines are created not only at frequency distance Ω_0, but on a very large band including regular sub structures.

Going back now to the spectra obtained in solitons differing by their size a (figure 11), we can explain the results as follows [17]: in the small size soliton, PM effects dominate SRWS effects for two additional reasons:

- the soliton intensity is high, and thus PM effects are large
- the SRWS intensity threshold is smaller than the soliton intensity. Though this fact allows the development of a Stokes lines at $\Omega_0 = 2.3$ cm^{-1} of the laser line, it does not allow the large spectral broadening characteristic of the four photon SRWS processes because we are not in a collimated beam.

In contrast, in large size soliton, SRWS effects dominate phase modulation, particularly when I_s and I_T are close.

4. Polarization properties

In all the experiments described above, the input beam is linearly polarized, either TE or TM. In these cases, the polarization is maintained in the soliton. We change now the direction of the linearly polarized input electric field. Its angle θ with the *y* direction – i.e., with the TM electric field – can be varied between $\theta = 0$ and $\theta = 90°$, meaning respectively TM and TE incident polarizations. Whatever the input polarization state, the soliton power remains defined as the input power that is necessary to produce an output beam that has the same size as the input beam. We study the influence of θ on the spatial spectral and polarization properties of the output beam around the soliton power.

In figure 12 [24] the intensities I_{TE} and I_{TM} of the two output polarization components measured in the center of the beam $(x = y = 0)$ are presented as functions of input power P for five values of θ in the interval $0^\circ < \theta < 10^\circ$. The results lead to the following main conclusions:

- for $\theta = 0^\circ$ (pure TM entrance) the output beam is TM polarized
- when θ is increased, even if it remains small, a TE component develops quickly in the output beam, whereas the TM component decreases.

Figure 13 illustrates the situation at the soliton power: the ratios I_{TM}/I_S and I_{TE}/I_S are shown as functions of θ. The curves confirm that the TE intensity increases with θ much faster than expected from a purely linear behaviour obeying the Malus law and the TM intensity decreases simultaneously. So, the presence of even a small TE component at the

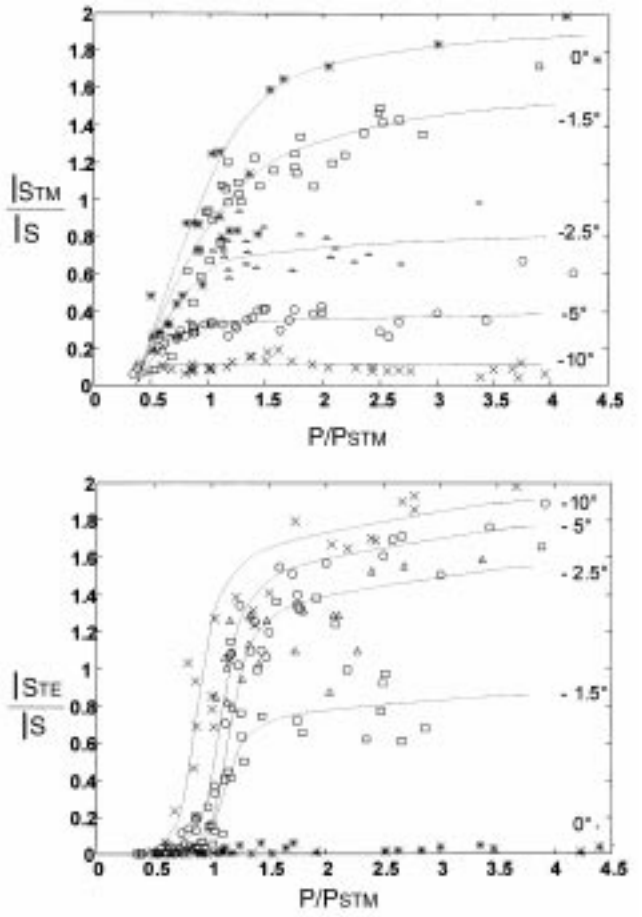

Figure 12. Intensity measurements I_{TE} and I_{TM} of the two output polarization components measured in the center of the beam $(x = y = 0)$ as a function of input power P for five values of θ in the interval $0^\circ < 10^\circ$.

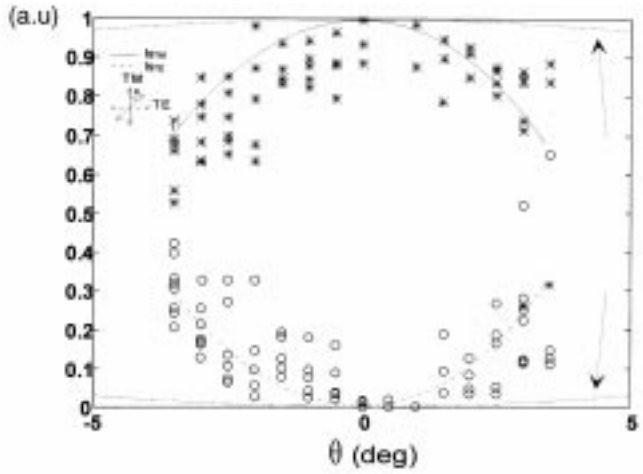

Figure 13. Ratios I_{TM}/Is and I_{TE}/Is, where Is is the intensity in the soliton and I_{TM} (asterisks) and I_{TE} (open circles) are, respectively, the intensities of the TM and the TE components, shown as a function of θ.

entrance of the guide tends to transform the output polarization into a TE polarization. Only the pure TE and TM modes retain their polarization in the soliton. We remark that this can explain the fluctuations noted above in the TM soliton power, caused by small imprecision on the y polarization.

Evolution of the TE and TM component sizes with power P for various values of θ are shown in figure 14. At soliton power $P = Ps$, and as soon as $\theta > 2^\circ$, the TE component has a size smaller than the soliton size, while the TM component resits focusing. For instance, at $\theta = 10^\circ$, the size of the TE component has reached the limit value of 20 μm.

From the measurements of intensities and sizes, it is possible to show that an energy exchange exists from the TM to the TE component, which is obviously confirmed by the total disappearance of the TM component for $\theta \geq 10^\circ$. This can be explained with help of the propagation equations writen for the two polarizations x, y. Equation (4) yields:

$$i\frac{\partial E_x}{\partial z} = -\frac{1}{2k_x}\frac{\partial^2 E_x}{\partial x^2} - A|E_x|^2E_x - B|E_y^2|E_x - CE_yE_yE_x^*\mathrm{e}^{-2i\Delta kz} \tag{23a}$$

$$i\frac{\partial E_y}{\partial z} = -\frac{1}{2k_y}\frac{\partial^2 E_y}{\partial x^2} - A|E_y|^2E_y - B|E_x^2|E_y - CE_xE_xE_y^*\mathrm{e}^{+2i\Delta kz} \tag{23b}$$

where E_x and E_y are the (x, y) components of the electric field, k_x and k_y the propagation constants of the orthogonal modes and $\Delta k = k_x - k_y$. A and B are complex coefficients proportional to the corresponding components of the third order susceptibility tensor. For molecular reorientation effects (case of CS_2), real parts of these coefficients obey $\mathscr{R}(A) = kn_2H$, and $\mathscr{R}(B) = \mathscr{R}(A)/4, \mathscr{R}(C) = 3/4\mathscr{R}(A)$.

In eqs (23) we remark the presence of two kinds of crossed terms (proportional to B and C) able to mix E_y and E_x field components. If A, B and C are real, i.e., if nonlinearities are only of the refractive index type, and if $\Delta k = 0$, the terms proportional to B and

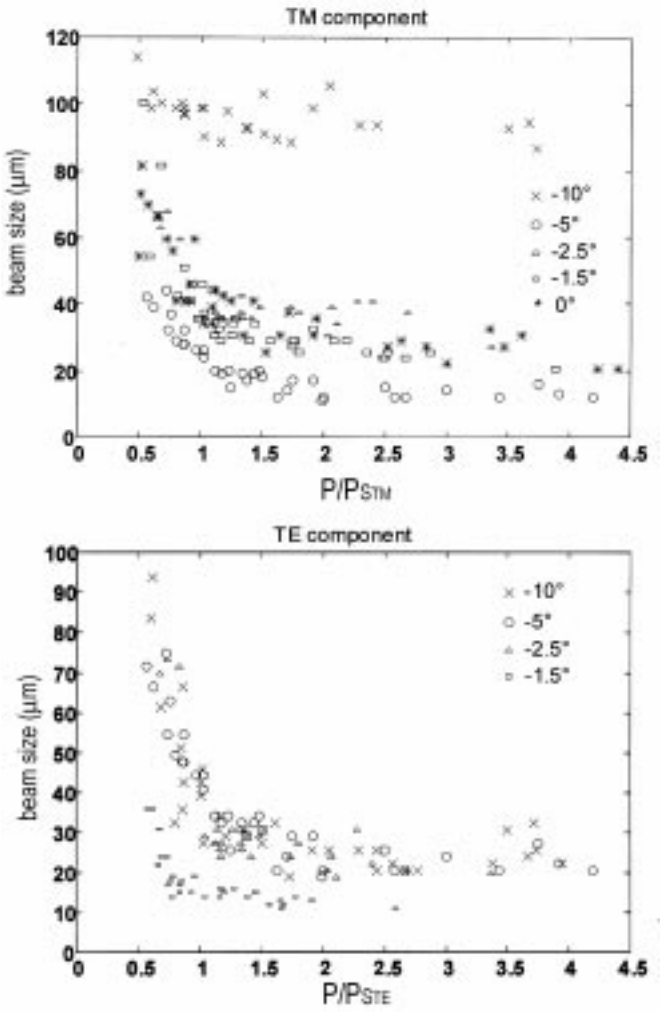

Figure 14. Output beam sizes of the TE and TM components as a function of the input beam power for five values of θ.

C cannot be the source of energy exchanges between the orthogonal field components. However, if $\Delta k \neq 0$, terms proportional to C yield energy exchanges between cross polarized modes (in order to verify these affirmations one can calculate from eq. (23) $\partial I_x/\partial z = (H\partial[E_x E_x^*]/\partial z)$, and $(\partial I_y/\partial z)$).

In isotropic bulk material propagation, there are no spatial dissymetries and thus $\Delta k = 0$. But in a planar waveguide it is known (24) that the TE and TM modes propagate in the z direction with different phase velocities. In our waveguide case, TM modes propagate faster than TE modes and thus $\Delta k > 0$.

The existence of $\Delta k \neq 0$ implies that the polarization state of the electric field changes all along its guided propagation, except for the pure TE and TM modes. However, in a linear

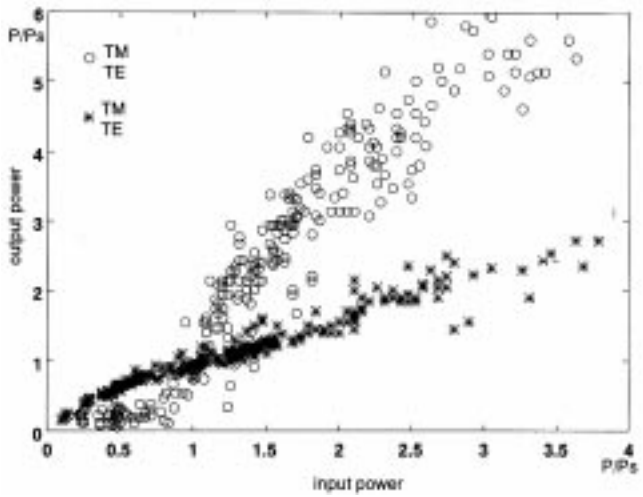

Figure 15. TE and TM output power versus input power for $a = 50\ \mu$m, $\theta = 2^\circ$ ($R_0 = 10^{-4}$).

planar waveguide polarization changes are not accompanied by energy exchanges between orthogonal modes. Nonlinear terms proportional to C in equations 23 are the source of an energy transfer from the TM mode to the TE mode when the signs are those of our experiments, ie $C > 0$ and $\Delta k < 0$.

It is thus clear now that the use of a nonlinear planar waveguide allows energy transfers between crossed polarized field components. This property can be used in applications for polarization switching, as it is demonstrated in figure 15. Several questions arise now: is the observed inter-mode energy exchange sufficiently reproducible, to be used in applications? How does it depend on the spatial characteristics d and a and on the value of n_2? When entrance power is varied does it change progressively or suddenly? Does the soliton power play a particular role? We answer these questions in the next section.

5. Polarization switching control

In order to characterize the polarization switching, we define the ratio R of the output powers in the two orthogonal directions TE, TM: $R = (P_{\mathrm{TE}}/P_{\mathrm{TM}})$. The input value of R is $R_0 = tg^2\theta$. We have measured the ratio R as a function of input power P for different sizes of the waveguide. Typical results are presented in figure 16. The first observation is that R can reach very large values: for instance, with $R_0 = 0.03$, R takes values far larger than 1. The power P_p for which $R = 1$, that can be considered as a performance index of the switch is always of the order of the soliton power P_s: in all the size combinations tested (d varying from 8 to 12 μm, a from 40 to 120 μm), the value P_p/P_s is in the range 0.6 to 0.8. This yields $R = 1$ at power levels of some hundreds of watt. Results are reproducible. However, if P is increased far above $2P_s$, oscillations of R can be observed in some waveguides

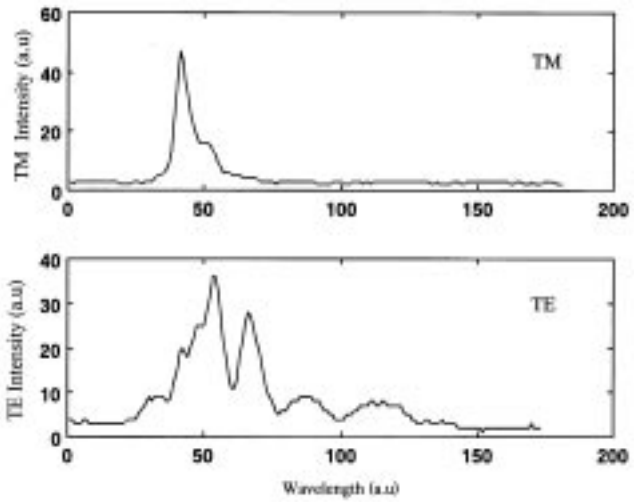

Figure 16. Spectra of the TE and TM components for $\theta = 10°$ ($R_0 = 0.03$), $a = 120\ \mu$m, $d = 12\ \mu$m, $P = 1.02P_s$.

(this is due to the presence of terms $e^{\pm 2i\Delta kz}$ in eqs (23)). Moreover, presence of SRWS near its threshold can create fluctuations in the value of R. As we shall see later, presence of SRWS enhances R, and thus fluctuations carried by its presence are not dangerous in switching applications.

Observations of spectral properties of the two components TE, TM reserve surprising results: the TE component spectrum is much larger than the TM one [21,25]. Figure 16 illustrates this difference. Whatever the cause of spectral broadening – i.e., phase modulation or scattering – the TE spectrum around the soliton power is always larger than the TM one. In fact, phase modulation and scattering occur only in the TE mode. In this mode, the spectral Stokes wings have a smaller spatial size than the undisplaced laser frequency [7]. This contribute to explain why – all wavelengths being mixed – the TE mode has a smaller spatial size than the TM one (see above, figure 14).

But probably, the main surprising result consists in the improvement of the switching efficiency by the presence of the spectral broadening. Figure 17 shows clearly this result. The value of R as function of the incident power P is represented in two waveguides ($a = 80\ \mu$m, $a = 120\ \mu$m) and the measurement points obtained around the SRWS threshold are classified in three groups, corresponding either to absence of PM and SRWS (at low intensities), or to presence of one or two of these phenomena. We take the opportunity of the fluctuations of the SRWS intensity near its threshold to make measurements of R in the presence or absence of SRWS for a same value of P. Results (figure 17a) show clearly that R is strongly enhanced by the presence of SRWS. The value of R is multiplied by a factor of the order of 2 when SRWS is created. The reason of the enhancement of energy transfer from TM to TE mode by SRWS is due to the presence of supplementary coupling terms in eqs (23). These terms are of the general following type:

$$i\frac{\partial E_x^S}{\partial z} + E_x^L E_x^L E_y^{*AS} e^{-i\Delta k' z} \tag{24}$$

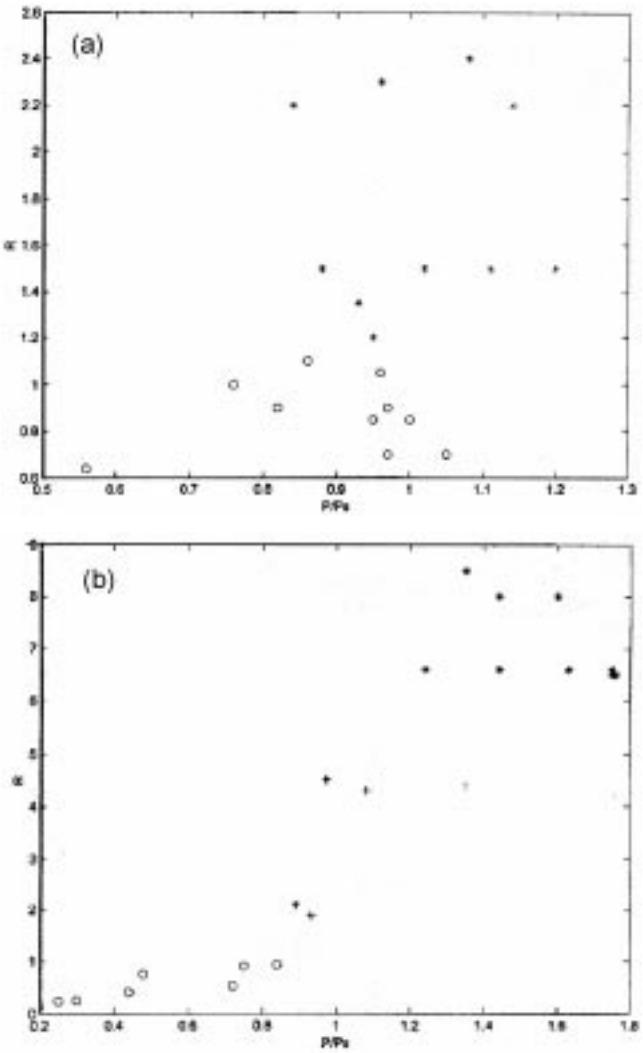

Figure 17. Values of $R = (P_{\mathrm{TE}}/T_{\mathrm{TM}}$ versus P/Ps, for $R_0 = 0.03$. (**a**) $d = 12\ \mu$m, $a = 120\ \mu$m; (**b**) $d = 12\ \mu$m, $a = 80\ \mu$m; o : points without PM and SRWS, * : points with SRWS, + : points with PM, without SRWS.

where E_i^L, E_i^S, E_i^{AS} are the laser, Stokes and anti-Stokes fields in the ith direction, and where:

$$\Delta k' = 2k_{Lx} - k_{Sy} - k_{ASy}$$

In eq. (24), $\Delta k'$ plays the same kind of role as Δk in eq. (23). Calculation of $\Delta k'$ shows that it has the same sign as Δk, and that $|\Delta k'| > |\Delta k|$: the coupling term between TM and TE directions is enhanced by the presence of FP SRWS process.

The same ideas and calculations can be developed concerning the role of PM in polarization switching: the symmetrical $S-AS$ spectral broadening it provides helps the energy transfer from TM versus TE.

A general conclusion resulting of the detailed spectral observations in the TE and TM components is that polarization switching from TM to TE mode is strongly enhanced by the spectral broadenings due to the presence of phase modulation and stimulated scatterings. There is a cumulative effect of two processes: at low powers, energy transfer from TM to TE is due to the phase velocity difference between orthogonal modes created by the guiding structure in the nonlinear medium. Then, when soliton power or/and stimulated scattering thresholds are reached, spectral broadenings reinforce strongly the phase velocity difference initially created, and this yields larger inter mode energy transfers.

If we go back now to the questions concerning the qualities of the polarization switch in view of applications:

1. the CS_2 waveguide provides large values of R, seeming much larger than those reported for instance in solid AlGaAs waveguides [26].
2. Reproducibility is sufficient, in term of extinction of the TM beam to the benefit of the TE beam.
3. A rather abrupt increase of the slope $R = f(P)$ is observed around the soliton power, due to contributions of phase modulation and scattering.

All the previous results, obtained with CS_2, have been verified with other liquids, such as C_6H_6 and $CHCl_3$. In $CHCl_3$, where $n_2 = 0.3\ 10^{-18}$ m^2/W, P_s is ten times larger than in $CHCl_3$ for the same values of (d, a), as expected from eq. (15). There is no SRWS (no anisotropy of the molecule), but stimulated Raman scattering SRS has a threshold $I_T \approx 15$ GW/cm^2, in the range of the value of I_s when $a = 30\ \mu$m. Polarization switching is observed too, and SRS plays a role in the stabilization of the value of R when the entrance power is increased [27].

6. Conclusions

Experimental study of the propagation of light in a planar waveguide filled with a liquid displaying a nonlinear refraction index confirms the model of the bi-dimensional spatial soliton. Polarization effects open the door to applications, particularly to optical switching, to control of an intense beam by a weak beam and to power limiting. Stimulated Rayleigh and Raman scatterings, together with phase modulation that occurs in the case of short laser pulses, yield spectral changes and contribute strongly to polarization changes.

References

[1] R W Boyd, *Nonlinear Optics* (Academic press, New York, 1992) p. 257
[2] S A Akhmanov, R V Khoklov and A P Sukhorukov, in *Laser handbook* edited by F T Arecchi and E O Schulz-Dubois (North-Holland, Amsterdam, 1972) vol. 2
[3] F Shimizu and B P Stoicheff, Study of the duration and birefringence of self-trapped filaments in CS_2, *IEEE J. Quant. Elec.* **5(11)**, 544 (1969)
[4] J Reintjes, R L Carman and F Shimizu, Study of sel-focusing and self-phase modulation in the picosecond time regime, *Phys. Rev.* **A8(3)**, 1486 (1973)

[5] G Rivoire, C Desblancs, J L Ferrier, J Gazengel and N Phu Xuan, Propagation in media with Raman type nonlinearity: polarization states of the waves and gains, *Opt. Quant. Elec.* **15**, 209 (1983)
[6] M Vampouille, B Colombeau and C Froehly, Application du contrôle de l'autofocalisation dans CS2 au racourcissement d'impulsions laser picoseconde, *Opt. Quant. Elec.* **14**, 253 (1982)
[7] M Lefkir and G Rivoire, Influence of transverse effects on measurements of third order nonlinear susceptibility by self-induced polarization state changes, *J. Opt. Soc. Am.* **B14**, 11, 2856 (1997)
[8] O Rahn and M Maier, Raman limited beam diameters in self-focusing of laser light, *Phys. Rev.* **A9**, 3, 1427 (1974)
[9] J Gazengel and G Rivoire, Spatial structure of a picosecond laser beam in a nonlinear medium, *Optica. Acta* **26**, 4, 483 (1979)
[10] V E Zakharov and A B Shabat, Exact theory of two dimensional self-focusing and one-dimensional self-modulation of waves in nonlinear media, *JETP* **34**, 62 (1972)
[11] A Barthelemy, S Maneuf and C Froehly, Stable self-trapping of laser beams: observation in a nonlinear planar waveguide, *Opt. Comm.* **55**, 201 (1985)
[12] J S Aitchinson, A M Weiner, Y Silberberg, M K Oliver, J L Jackel, D T Leavids, E M Vogel and P W E Smith, Observation of spatial optical solitons in a nonlinear glass waveguide, *Opt. Lett.* **15**, 9, 471 (1990)
[13] J S Aitchinson, J U Kang and G I Stegeman, Signal gain due to a polarization coupling in a AlGaAs channel waveguide, *Appl. Phys. Lett.* **67(17)**, 2456 (1993)
[14] S Maneuf, R Desailly and C Froehly, Stable self trapping of laser beams: observations in a nonlinear planar waveguide, *Opt. Comm.* **65**, 3, 193 (1988)
[15] O Graydon, Liquid waveguides speed up all-optical switching, in *Opt. Laser Europe*, p. 17, January 1999
[16] D Wang, R Barillé and G Rvoire, Stokes spectral broadening at an over soliton threshold excitation in a planar waveguide, *J. Opt. Soc. Am.* **B15**, 1, 181 (1998)
[17] R Barillé, J P Bourdin and G Rivoire, Instabilities due to Rayleigh wing scattering in a spatial soliton, *Opt. Comm.* **171**, 291 (1999)
[18] D Wang, R Barillé and G Rivoire, Influence of propagation of optical pulses on stimulated Rayleigh wing scattering in a Kerr medium, *J. Opt. Soc. Am.* **B14(10)**, 2584 (1997)
[19] S C Pinault and M J Potasek, *J. Opt. Soc. Am.* **B2**, 1318 (1985)
[20] W Kaiser and M Maier, in *Laser Handbook* edited by F T Arecchi and E O Schulz Dubois (North-Holland, Amsterdam, 1972)
[21] R Barille and G Rivoire, Stimulated Rayleigh Wing Scattering, *Nonlinear scattering, in Scattering* (Academic press, London, 2001)
[22] A Fahmi, J P Bourdin, R Chevalier, X Nguyen Phu and G Rivoire, Influence of stimulated Rayleigh wing scattering in χ^3 measurements and wave mixing experiments in CS_2, *Nonlinear Opt.* **12**, 165 (1995)
[23] R Barillé, S Sogomonian and G Rivoire, Spatial and spectral properties of SRWS pumped by a Bessel beam: role of four photon parametric processes, *J. Opt. Soc. Am.* **B16**, 7 (1999)
[24] S Huard, Polarisation de la lumiére (Ed. Masson, Paris, 1994)
[25] D Wang, R Barillé and G Rivoire, Influence of soliton propagation on the beam polarization dynamics in a planar waveguide, *J. Opt. Soc. Am.* **B15**, 11 (1998)
[26] L Friedrich, R Malendevich, G I Stegeman, J M Soto-Crespo, N N Akhmediev and J S Aitchison, Radiation related polarization instability of fast Kerr spatial solitons in slab waveguides, *Opt. Comm. 186*, 185 (2000)
[27] V Boucher, R Barillé and G Rivoire, Polarization changes in planar waveguide in the presence of stimulated scatterings (Rayleigh, Raman), *IQEC 2000, Nice* (*France*), 10–15 September (2000)